arXiv:1611.00165v1 [physics.ins-det] 1 Nov 2016

Alpha-event and surface characterisation in segmented true-coaxial HPGe detectors

I. Abt[a], L. Garbini[a,*], C. Gooch[a], S. Irlbeck[a], X. Liu[a], M. Palermo[a,1], O. Schulz[a]

[a] *Max-Planck-Institut für Physik, Munich, Germany*

Abstract

A detailed study of alpha interactions on the passivation layer on the end-plate of a true-coaxial high-purity germanium detector is presented. The observation of alpha events on such a surface indicates an unexpectedly thin so-called "dead layer" of less than 20 μm thickness. In addition, the influence of the metalisation close to the end-plate on the time evolution of the output pulses is discussed. The results indicate that alpha contamination can result in events which could be mistaken as signals for neutrinoless double beta decay and provide some guidance on how to prevent this.

Keywords: HPGe detectors, position-sensitive devices, neutrinoless double-beta decay, background-reduction techniques

1. Introduction

The search for neutrinoless double-beta ($0\nu\beta\beta$) decay is one of the most promising approaches to look for physics beyond the standard model. The germanium isotope ^{76}Ge is one of the candidates for such a search. The current generation of germanium experiments, GERDA [1] and the MAJORANA demonstrator [2], are already setting significant limits on the half-life of ^{76}Ge for $0\nu\beta\beta$ decay [3, 4] and are working hard to push the currently available technologies to reduce the background. Recently, the GERDA collaboration has presented limits on the half-life of 5.2×10^{25} y and on the mass of the coherent Majorana state, m_{ee}, between 160 and 400 meV, depending on the nuclear matrix element used. A background index of $\approx 10^{-3}$ counts/keV/kg/y was also presented. A commonly accepted goal is to increase the sensitivity down to 10 meV in order to cover the parameter space associated with the inverted hierarchy [5]. This requires a ton-scale experiment with a background index of better than 10^{-4} counts/keV/kg/y [6]. Surface contamination of the detectors with alpha emitters has to be considered for such an experiment [7].

Similar considerations lead also to the desire to build a ton-scale germanium experiment to search for dark matter [8, 9, 10]. While true-coaxial detectors are not candidates for

*Corresponding Author

Email address: luciagarbini86@gmail.com.mpg.de (L. Garbini)

[1] Now at Physics and Astronomy Department, University of Hawaii at Manoa, HI, US

such experiments, the relevant detectors still have passivated or oxydised surfaces and alpha interactions are relevant.

The choice of detector technology for any ton-scale detector needs careful consideration. The study presented here provides some input to the decision making process. Data are presented for which the passivated top surface of a specially designed true-coaxial germanium detector was scanned with a ^{241}Am source. The events induced by the alpha particles are characterised. It is shown how alpha particles can mimic $0\nu\beta\beta$ signal events by losing part of their energy in the so-called "dead layer" underneath a passivated surface. This layer forms in areas of a given detector where the electric field generated by the electrodes is not strong enough to fully deplete this region. The location and thickness of such a layer is determined by the detector geometry. In true-coaxial detectors, a known region for the formation of such a layer is below the passivated end-plates. The thickness of such layers can be measured by determining the energy loss of alpha particles.

The measurements presented here reveal such a dead layer, but also show that the picture of a clearly defined dead layer is too simplistic. Some of the charge carriers created are shown to be trapped along their paths to the collecting electrodes. In addition, the influence of the metalisation close to the end-plate under study is discussed.

2. Experimental setup

The measurements presented in this paper were performed operating the "Super-Siegfried" test-detector in the GALATEA test-facility [11, 12] shown in Fig. 1, located at the Max-Planck-Institut für Physik in Munich. GALATEA is based on a vacuum chamber in which germanium detectors can be scanned by a system of three motorised stages. Two tungsten collimators are used to focus the radiation onto the mantle and the top plate of any cylindrical detector. As the paths between the collimators and the detector are free of material, it is possible to use alpha sources.

The data presented in this work were taken with a 10 kBq ^{241}Am source, placed inside the collimator above the top end-plate. The radius of the beam spot was 1.8 mm. Also present was a 42 kBq ^{152}Eu calibration source, located in the collimator on the side of the detector. It was moved down as far as possible in order to minimise its influence on the measurement.

The isotope ^{241}Am emits alpha particles of about 5.5 MeV. However, the source is encapsulated. Separate measurements on the side of another germanium detector, where no significant dead layer exists, showed that the encapsulation reduces the mean energy of the alphas to 4.5 MeV with a Gaussian variation of 0.2 MeV [13]. The variation corresponds to a 10 % inhomogeneity of the thickness of the plastic encapsulation. The energy loss in germanium is 172 keV/μm. Thus, any observation of alpha interactions indicates that the dead layer is thinner than 26 μm.

The ^{241}Am source also produces gamma-rays of 59.5 keV which have a mean free path in germanium of about 0.9 mm. Thus, two different volumes can be probed with one source. However, the tungsten collimator also introduces k–α emission lines at 59.3 keV

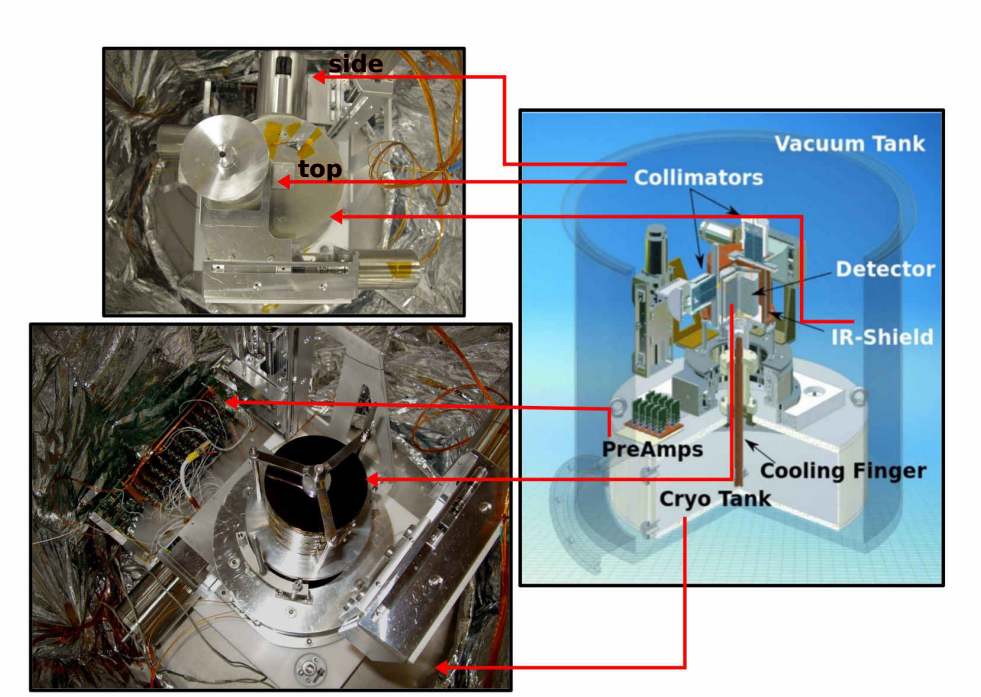

Figure 1: Operation of the Super-Siegfried detector in the GALATEA test facility, taken from [13].

and 58.0 keV which cannot be separated from the 59.5 keV gammas. They blur the beam spot such that the probed volumes not only differ in depth, but also slightly in radius.

Figure 2 shows the schematic of Super-Siegfried and the locations of the measurements. It is a cylindrical true coaxial n-type high-purity segmented germanium detector produced by Canberra France. It has a height of 70 mm. The radius of the inner bore hole is 5.05 mm and the outer radius is 37.5 mm. According to the manufacturer, the detector has a concentration of electrically active impurities between $\rho = 0.44 \times 10^{10}\text{cm}^{-3}$ at the top and $\rho = 1.30 \times 10^{10}\text{cm}^{-3}$ at the bottom of the detector. The full depletion voltage was determined to be 2250 V. The operational voltage was 3000 V.

The main part of the detector is segmented 6-fold in ϕ and 3-fold in z. Such a detector was characterised in detail previously [14]. An additional segment, 5 mm high and not segmented in ϕ, is located above the regular 18 segments. The signals from the detector were recorded as charge pulses. Charge carriers, electrons and holes created by an energy deposition, drift towards the electrodes. The electrons drift towards the core electrode and the holes towards the segment electrodes. During the drift they induce charges which are recorded. The amount of charge registered in a given electrode at a given time depends on the amount of charge carriers drifting and the strength of the so-called weighting field of the electrode. The weighting field of the core is strong close to the centre of the detector while the weighting field of the segment electrodes is strong close to the mantle.

Super-Siegfried was previously investigated using the 122 keV ^{152}Eu line with the detector mounted in a conventional cryostat [15]. The thin top segment, called segment 19, was designed to study events on the end-plate. As it is fairly thin, any charge drifting towards the segment 19 electrode also creates strong so-called mirror pulses in the segments underneath, which facilitate a detailed pulse-shape analysis.

For each event, the pulses for the core and all 19 segments were recorded with a 75 MHz sampling rate. All pulses were corrected offline for linear cross-talk and calibrated for energy. For the core and the collecting segments, the energy was determined after calibration as the height of the respective pulse using an asymmetric trapezoidal filter. Throughout the paper, the risetime of a pulse refers to the time for the pulse to develop from 10% to 90% of its pulse height.

The metalisation of the detector was reduced in order to study its influence on the properties of the detector [2]. Only a circular area with a radius of about 6 mm in the middle of each regular segment was metalised, see Fig. 2(c) . The metal contact of segment 19 only covered a sector of the mantle about 2 cm long.

Figure 3 depicts a schematic vertical cut through one half of segment 19. The presence of the passivation layer, the conical shape of the bore hole together with the geometry of the core electrode and the partial metalisation of segment 19, see Fig. 2(c) , determine the geometry of the weak and distorted electric field lines in this volume. There are volumes from which no charge carriers emerge and volumes in which charge carriers, electrons or holes, get trapped. The electrons drift towards the core through a region in which the weighting field of the core is much stronger than for the segment (mantle) electrode. For the holes, the situation is reversed. Their path towards the segment electrode is characterised by a strong segment weighting-field. Thus, the trapping of electrons (holes) affects predominantly the energy registered in the core (segment).

Generally, any region for which charge depositions cannot be registered, is called "dead" or "inactive". Previous measurements with ^{152}Eu [15] indicated that the inactive volume of the detector close to the bore hole is as thick as 5 mm. These measurements were not precise enough to evaluate the inactive volume at larger radii. The expectations [17] were that at larger radii, the thickness of the dead layer would be at least of the order of 50 to 100 μm.

3. Observation of alpha radiation

Contrary to expectations, alpha interactions were consistently observed for radii larger than 25 mm. Figure 4(a) shows the spectra recorded by the core and by segment 19 for $r = 26.0$ mm and $\phi = 118°$, a point covered by the AS01 scan, see Fig. 2(b) . The correlation between the energies recorded in the core and in segment 19 is shown in Fig. 4(b) .

Broad bumps, from now on referred to as alpha peaks, are dominating both the core and segment 19 spectra at energies above 2 MeV. The core spectrum also shows the charac-

[2] As aluminium is not completely radiopure a reduction of the metalisation would reduce any background from this source for low-background experiments [16].

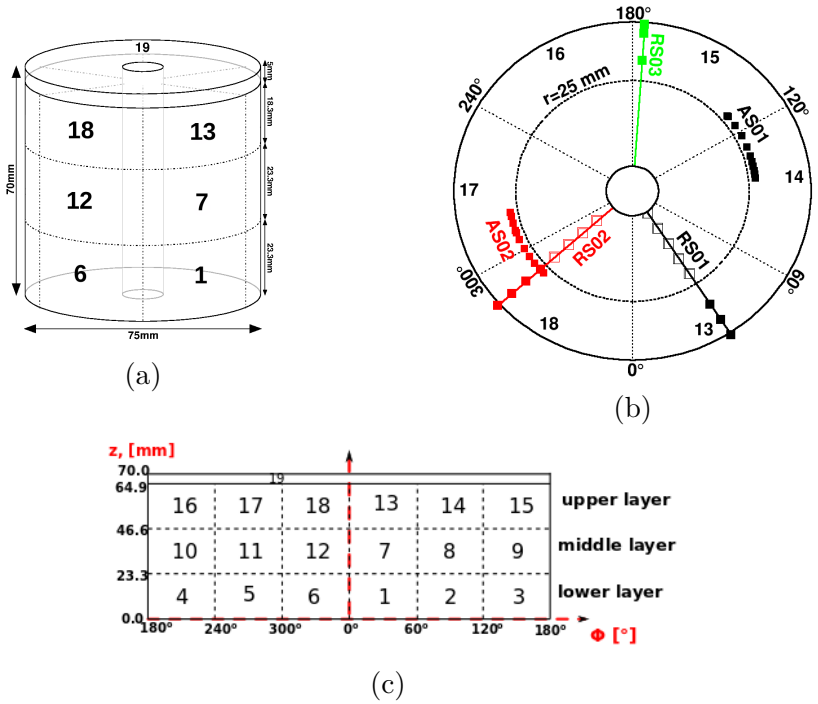

Figure 2: (a) Schematic of the 18+1 fold segmented Super-Siegfried detector, (b) the locations of the individual measurements on the top surface. The numbers indicate the segments underneath. Open symbols indicate no observation of alpha interaction at the probed location, (c) rolled out detector mantle with dimensions and reference system. The metalised contacts are indicated as shaded areas, adapted from [13]

teristic gamma lines due to natural radioactivity and due to the ^{152}Eu source. Segment 19 is too thin to fully absorb high-energy gammas with good efficiency, but the correlation plot, Fig. 4(b) , shows a thin line along the diagonal caused by single-segment 19 events. The 59 keV line is very clearly seen in both the core and segment 19 and its equal location confirms the validity of the energy calibration. Thus, the difference of the location of the alpha peaks has to be due to a different charge collection efficiency for electrons and holes. This indicates that holes must be trapped to explain the reduced energy observed on segment 19 as depicted in Fig. 4(a) .

The band in Fig. 4(b) associated with alpha events extends down to extremely low energies. However, at low energies, multi-segment events form a background to the alpha events. At the highest energies, where the band represents the distinct alpha peaks of Fig. 4(a) , basically no gamma background is present. High-energy alpha events were selected for further investigation by requiring single-segment 19 events with core (segment 19) energies, E_0 (E_{19}) of

$$\begin{aligned} E_{min}(\alpha_0^{peak}) < E_0 < E_{max}(\alpha_0^{peak}) \,, \\ E_{min}(\alpha_{19}^{peak}) < E_{19} < E_{max}(\alpha_{19}^{peak}) \,, \end{aligned} \tag{1}$$

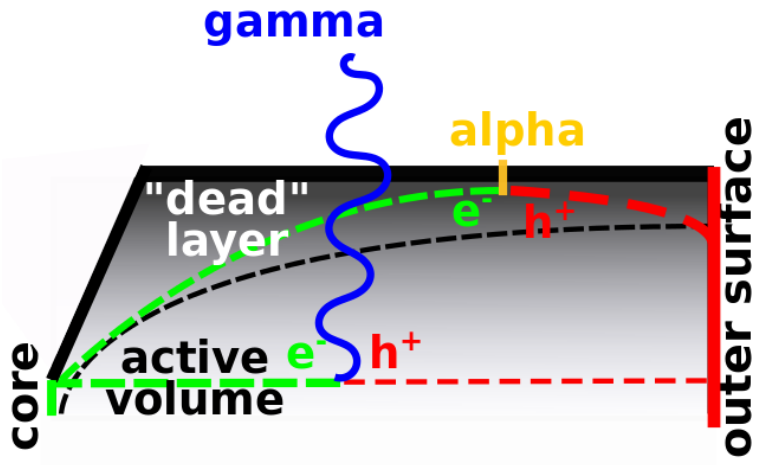

Figure 3: Vertical cut through the top of one half of the Super-Siegfried – not to scale. The central hole opens conically; the core electrode does not cover this surface. It is passivated like the top of the detector. The mantle electrode extends to almost the top of the detector. An alpha and a gamma interaction are indicated. A dead layer forms underneath the passivation. At larger radii, alpha interactions are observed, even though the drift paths are not straight for charge carriers in this region, adapted from [13]

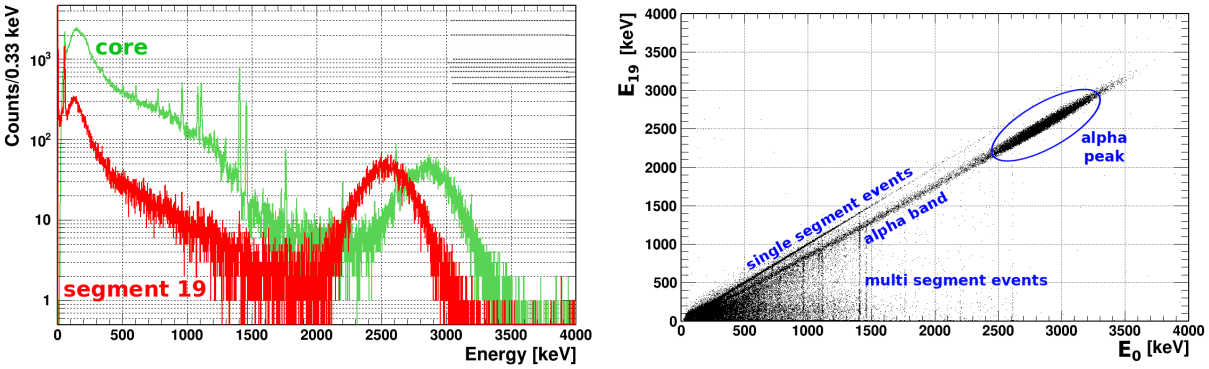

(a) (b)

Figure 4: Observation of alpha interactions during the scan AS01, see Fig. 2(b) , at r= 26.0 mm and $\phi = 118°$: (a) spectra recorded for the core and segment 19, (b) correlation between core and segment 19 energies, adapted from [13]

where $E_{min}(\alpha^{peak}_{0(19)})$ and $E_{max}(\alpha^{peak}_{0(19)})$ are defined as the three standard deviation differences from the mean as determined in respective Gaussian fits. The background from multi-site gamma events was measured to be much less than one percent for this selection

and not considered further.

4. Charge trapping

Figure 5 depicts a typical event selected according to Eq. 1 from the measurement AS01 at r= 26 mm and ϕ =118 °. The pulses from the core (top left), from segment 19 (top right) and from the 6 regular segments below are shown in the same time range and on the same energy scale. The rest of the detector did not show any activity.

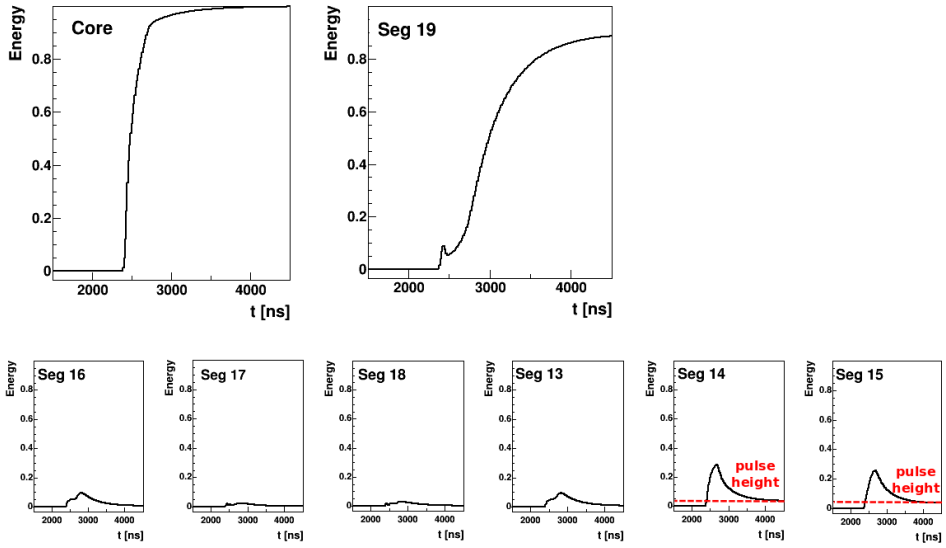

Figure 5: The pulses from the core (top left), segment 19 (top right) and the 6 regular segments below of a typical alpha event from the measurement at r = 26.0 mm and ϕ = 118°, in the AS01 set, close to the boundary between segments 14 and 15, adapted from [13].

The core[3] and segment 19 pulses look as expected for collecting electrodes. The segment 19 pulse does not reach the height of the core pulse and it is significantly slower[4]. The core pulse shows a clear kink around 2700 ns, indicating the end of the collection of electrons. The slow rise afterwards is caused by the slow drift of holes towards the mantle. All segments in the upper layer show positive mirror pulses. As these segments do not collect any charge, the pulses should return to the baseline. This happens for segments 13, 16, 17 and 18. The pulses from segments 14 and 15, directly underneath the interaction point, however, stay above the baseline; they are so-called truncated mirror pulses. This is

[3]The pulse was inverted for easier visual comparison.

[4]The small extra peak at the start of the pulse is an artefact created by the cross-talk correction which does not take differential cross-talk from the core into segment 19 into account. Such artefacts do not influence any of the results in this paper. Differential cross-talk occurs due to the very different risetimes of the core and segment 19 pulses.

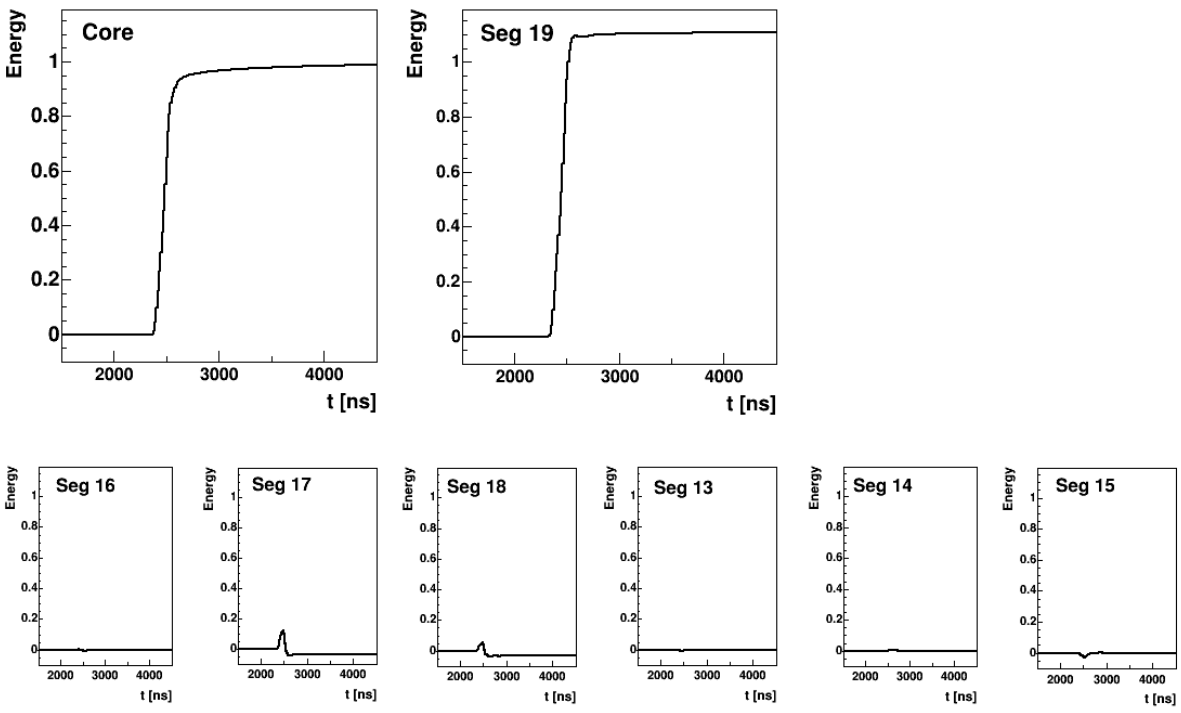

Figure 6: The pulses from the core (top left), segment 19 (top right) and the 6 regular segments below of a typical alpha event from the measurement at $r = 38.0\,\mathrm{mm}$ and $\phi = 312°$, in the RS02 set, close to the boundary between segments 17 and 18, adapted from [13].

the signature of charge trapping, where the amount of charge trapped is measured as the final height above the baseline, recorded as the pulse-height for a non-collecting segment. Adding the energies corresponding to the pulse-heights of the truncated mirror pulses to the energy measured in segment 19, the energy corresponding to the core pulse is recovered. For this source position, 100 % of the selected alpha-induced events contain such truncated positive mirror pulses; the pulses are very reproducible. The segment 19 pulse has not completely flattened out at the end of the recorded time window. It is possible that some holes were released later. The time window was unfortunately limited by the data acquisition system.

The absence of negative truncated mirror pulses at this position does not exclude that also electrons are trapped. As the holes drift outwards, they come closer to the segment electrodes than the electrons and thus the large positive charge they induce makes the observation of a smaller amount of induced negative charge indicating electron trapping impossible.

The trapping of holes is not due to the conditions at the location where the electron-hole pairs are created. The long pulse shown for segment 19 in Fig. 5 shows that the reduced field underneath the top plate along which the holes drift causes the non-collection of holes.

At larger radii, also electron trapping was observed. Figure 6 shows an event at $r =$

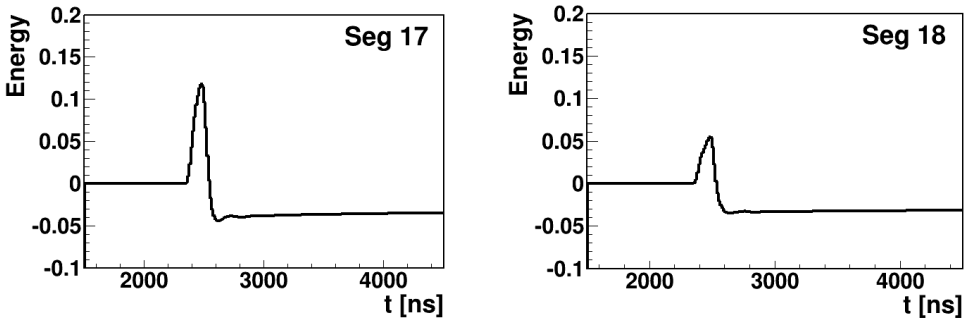

(a) (b)

Figure 7: Enlargement of the pulses from the event in Fig 6: (a) segment 17, (b) segment 18.

38.0 mm from RS02. This event is located at the edge of the detector and close to the sector of metalisation. Figure 6 top right shows that the energy collected in segment 19 is larger than in the core and that the drift of the holes is fast in this region. The mirror pulses in segments 17 and 18 shown in Figs. 7(a) and 7(b) first reflect the drift of the positive holes and then the drift of the electrons. They are trapped at $t \approx 2600$ ns. A very slow release of electrons is indicated by the slow rising tails of the mirror pulses and the steady increase of the core pulse at $t > 2600$ ns.

5. Location dependence of charge trapping

Figure 8 shows the correlation between the energy in segment 19, E_{19}, and the energy in the core, E_0, for the three different radii probed by the RS01 set as introduced in Fig. 2(b) .

With increasing radius, the alpha band moves from below the diagonal, normally indicating single segment events, to above. The core registers more energy for small radii and segment 19 registers more energy for large radii, close to the edge of the detector. The change in observed core energy suggests that either the really inactive volume of the detector becomes thicker towards larger radii or that also electrons get trapped. As the energy observed in segment 19 increases, the latter explanation is more consistent. This agrees also with expectations. As the radius increases, the path of the electrons becomes longer and they are more likely to enter the volume around the bore hole. The situation is reversed for holes. Their path shortens and their trapping becomes less probable.

In order to systematically study the radial dependence of charge trapping, truncated mirror pulses were methodically searched for. For all positions and selected alpha events, the pulses of the segment underneath the interaction zone were classified [13]. The fractions $f_\alpha^{\rm pt}$ of pulses falling into six "pulse types"(pt), "mirror positive", "mirror truncated positive", "mirror negative", "mirror truncated negative", "normal collecting" and "no activity", were calculated. Figure 9 shows $f_\alpha^{\rm pt}$ as a function of the radius for the three different azimuthal angles associated with the scans RS01, RS02 and RS03. The results are very

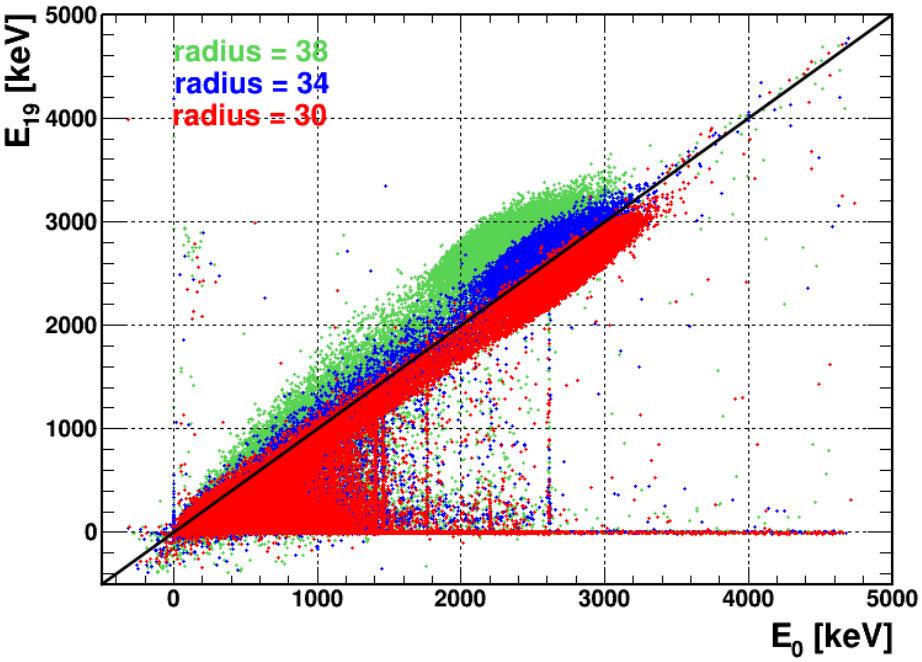

Figure 8: Correlation between E_0 and E_{19} for measurements at different radii at $\phi = 33°$, RS01, see Fig. 2(b). The line along the diagonal indicates $E_0 = E_{19}$, taken from [13].

consistent at the different angles. Up to $r = 30\,\text{mm}$, all events show positive truncated mirror-pulses, indicating hole trapping. At $r = 34\,\text{mm}$, the fractions of positive truncated mirror-pulses drops and negative truncated mirror-pulses become observable. At the edge of the detector, negative truncated mirror-pulses dominate, indicating electron trapping. The radial dependence of the effect is the same for RS02 close to the metalisation as for the other scans.

The results obtained for the two azimuthal scans AS01 and AS02 at $r = 26\,\text{mm}$ and $r = 30\,\text{mm}$ confirm the results of the radial scans. For both scans, 100 % of the events contain positive truncated mirror-pulses in the respective segments underneath segment 19.

Truncated mirror pulses were also searched for in gamma events at the scan positions where alpha events were observed. None were found. This confirms that charge trapping is restricted to charge carriers created very close to the surface.

The observed energies in the core and segment 19 were converted into "effective dead layers" with "effective thicknesses"

$$\text{DL}_i^{\text{eff}} = \left(\frac{dE}{dx}\right)^{-1} (E^{\text{ini}} - \mu_i) \tag{2}$$

where $i = 0$ or 19, E^{ini} is the average incident alpha energy and μ_i is the observed average energy for the selected alpha events. This assumed that the energy observed is related

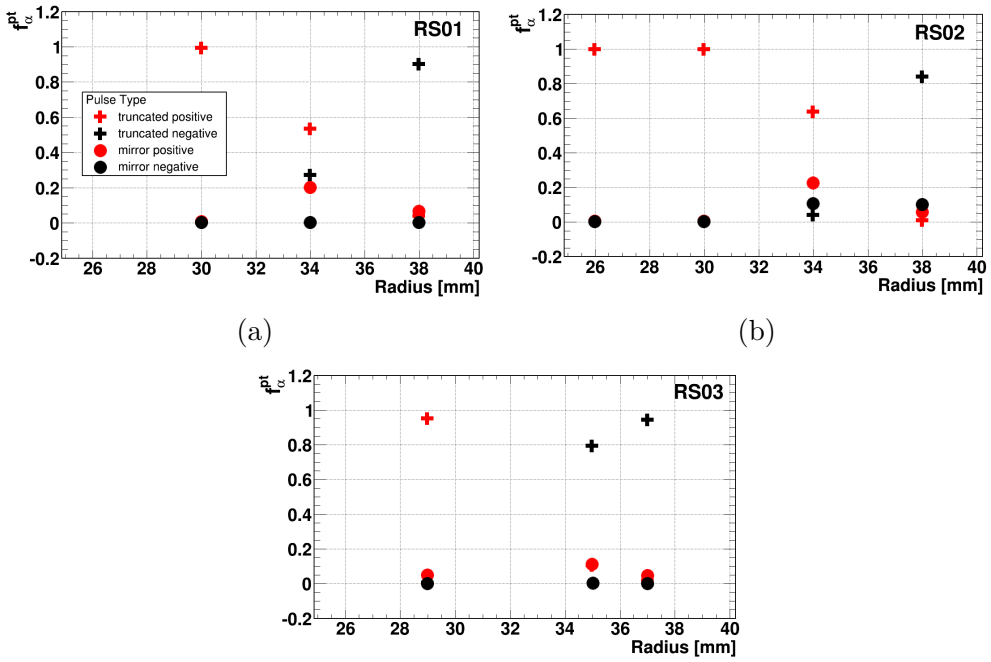

Figure 9: f_α^{pt} as a function of the radius for different azimuthal angles: (a) $\phi = 33°$, RS01, (b) $\phi = 312°$, RS02, (c) $\phi = 176°$, RS03, taken from [13].

to the energy lost in an inactive volume of the detector. This is clearly not the case as energy is also lost due to charge carrier trapping. However, for an experiment which only records energies, this is a convenient and common nomenclature. The results are depicted in Fig. 10 .

Corresponding to the decrease of observed energy in the core at increasing radii, $\mathrm{DL}_0^{\mathrm{eff}}$ slightly increases, see Fig. 10(a) . The situation for the holes, see Fig. 10(b) , is reversed. The conditions are very similar for all three radial scans. At $\phi = 176°$, the values of $\mathrm{DL}_0^{\mathrm{eff}}$ and $\mathrm{DL}_{19}^{\mathrm{eff}}$ at $r = 29\,\mathrm{mm}$ are slightly larger than for the other locations. This area is far away from the metalisation. However, the area covered by the azimuthal scan AS01 from $\phi = 95°$ to $\phi = 130°$ at $r = 26\,\mathrm{mm}$ is equally far away from the metalisation and does not show thicker effective dead layers. The values are $\mathrm{DL}_0^{\mathrm{eff}} \approx 10\,\mu\mathrm{m}$ and $\mathrm{DL}_{19}^{\mathrm{eff}} \approx 12\,\mu\mathrm{m}$ and are quite constant, see Fig. 11(top row).

The scan AS02, close to RS02 and covering the metalisation at $r = 30\,\mathrm{mm}$, revealed a shallow dependence on ϕ of both $\mathrm{DL}_0^{\mathrm{eff}}$ and $\mathrm{DL}_{19}^{\mathrm{eff}}$, see Fig. 11(bottom row). At the centre of the metalisation, both drop to about $10\,\mu\mathrm{m}$. It should be noted again that $\mathrm{DL}_0^{\mathrm{eff}}$ and $\mathrm{DL}_{19}^{\mathrm{eff}}$ are just a convenient nomenclature. The drop is more likely due to less charge trapping. The smallest value of $\mathrm{DL}_0^{\mathrm{eff}}$ could indicate a truly dead layer. But this is also rather unlikely. In Figs. 4(b) and 8 , events with observed energies in the core and segment 19 well above the alpha peaks are visible. Thus, there are events in which the charge carriers escape and

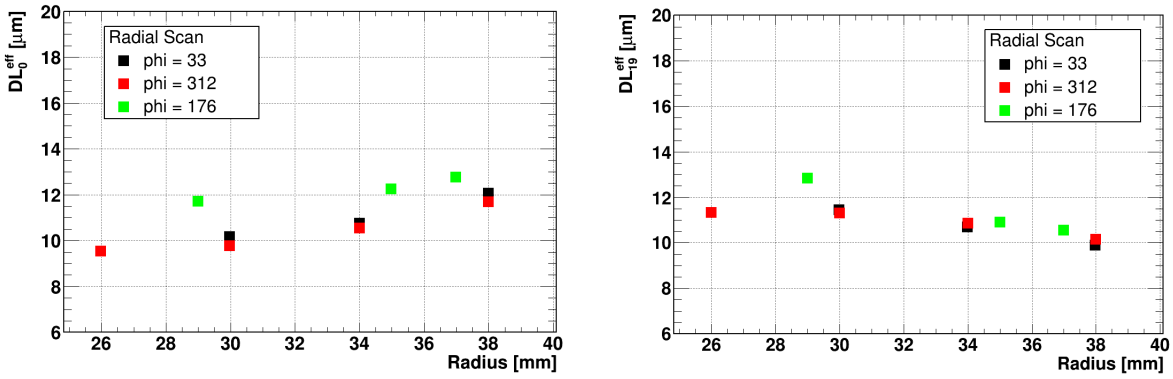

(a) (b)

Figure 10: Effective dead layer thicknesses, DL_i^{eff}, as a function of the radius for (a) the core, $i = 0$, and (b) segment 19, $i = 19$. The statistical uncertainties as determined by the fitting procedure are smaller than the symbol size, adapted from [13].

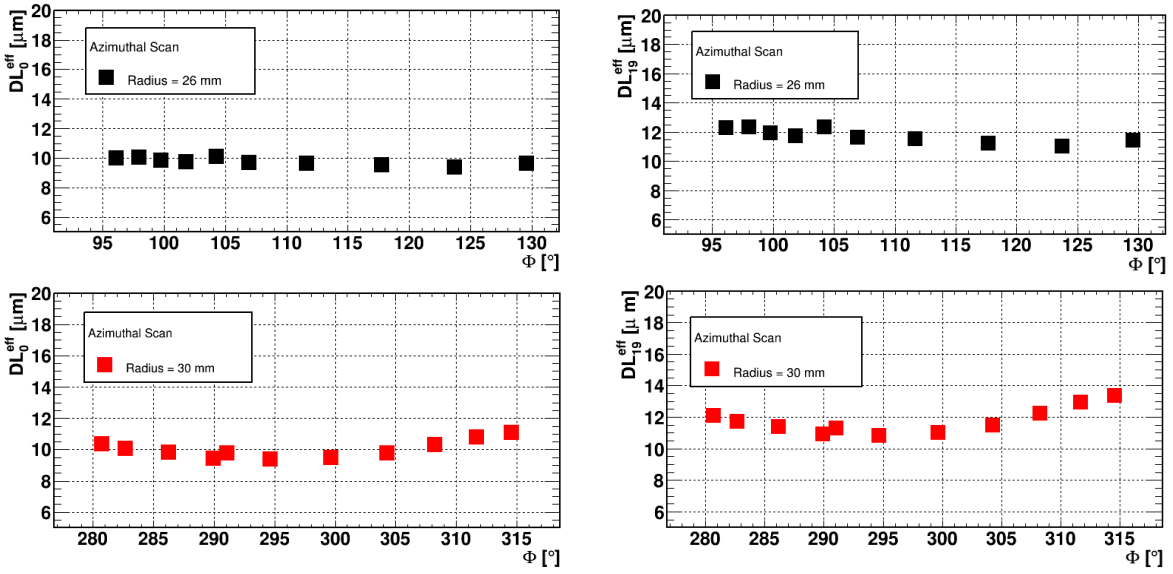

(a) (b)

Figure 11: Effective dead layer thicknesses, DL_i^{eff}, as a function of the azimuthal angle for (a) the core, $i = 0$, and (b) segment 19, $i = 19$. The statistical uncertainties as determined by the fitting procedure are smaller than the symbol size, adapted from [13].

make it all the way to the electrodes. On the other hand, the bands also extend to very low observed energies. For these events, almost all charge carriers cannot be collected, even though they were generated down to 26 μm. The events in the observed alpha peaks

are very reproducible. However, the other events cover a large phase-space of observed energies.

In general, the situation is quite similar at all locations where alpha interactions were observed. Alpha-dedicated measurements were also performed at radii smaller than 25 mm, see Fig. 2(b). However, alpha peaks were not observed anywhere for these smaller radii. The thickness of the inactive volume of the detector is rapidly growing in this region. This was also previously observed by probing with low energy gammas [15].

6. Risetimes of pulses

The risetime of pulses, RT_i^{10-90}, presented and discussed here always denotes the time in which the pulse rises from 10 % to 90 % of its amplitude. As the pulses recorded for the core are very different than for segment 19, this results in very different risetimes. The distributions of the risetimes for the radial scan RS01 are shown in Fig. 12.

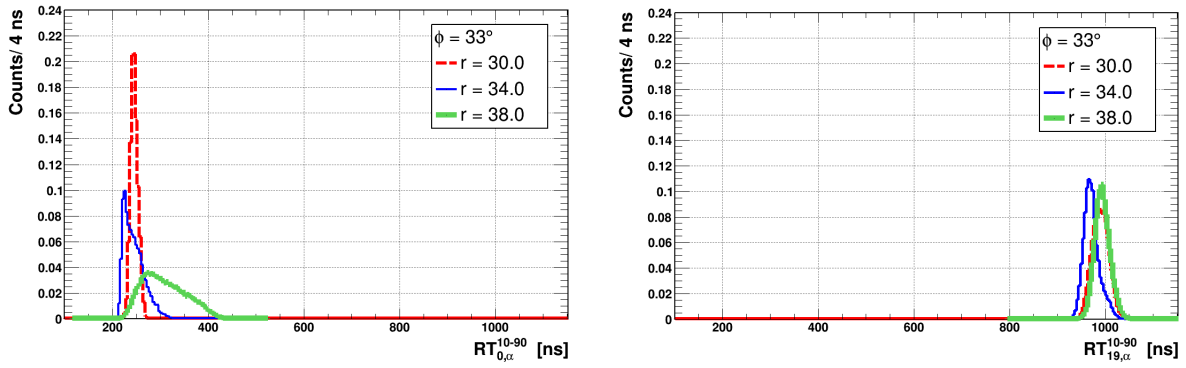

(a) (b)

Figure 12: Distribution of risetimes (a) RT_0^{10-90} for the core and (b) RT_{19}^{10-90} for segment 19 for the radial scan RS01, adapted from [13].

The pulses recorded in segment 19 rise much slower than the core pulses. This is possible because the holes drifting close to the mantle contribute little to the core pulse as the core weighting field is small in this region. The pulses in segment 19 are extremely long. The length of the expected drift path does not seem to be the determining fact, but rather the passage through a volume where the holes drift extremely slowly. The situation is different for the core pulses. They get longer for larger radii in accordance with the longer drift path.

The mean values of the risetime distributions of alpha events are shown for the two azimuthal scans in Fig. 13(a). The core pulses have average risetimes of slightly less than 300 ns for both scans. The average risetimes of the segment 19 pulses are however very different for the two scans. In the sector around the metalisation, the segment 19 pulses rise almost as fast as the core pulses. This indicates that the electric field is significantly

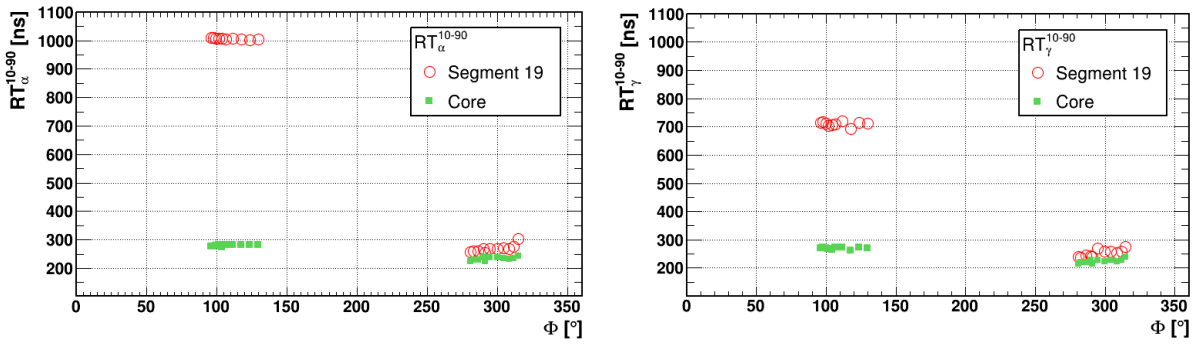

(a) (b)

Figure 13: Azimuthal dependence of the average RT^{10-90} for the core (square) and segment 19 (open circle) for (a) selected alpha events, (b) 59.5 keV gamma events.

stronger underneath the metalisation than in the outer region of the detector in other sectors.

Figure 13(b) shows the average risetimes for 59.5 keV gamma events. These gammas almost probe the complete volume of the top segment. Some gammas interact close to critical areas of the detector, where the charge collection is extremely slowed down. Some gammas, however, interact far away from such critical area. This causes extremely broad risetime distributions. The mean of these distributions lies significantly above the mean of the core distributions for the sector far away from the metalisation. This indicates that the weakening of the field is not restricted to the very thin layer probed by alpha particles.

This is confirmed by a side-scan of segment 19 which was performed earlier [15] in the K1 [14] vacuum cryostat. A 42 kBq collimated ^{152}Eu source was rotated around the detector at $z = 67.5$ mm, the middle of segment 19 (see 2(c)), in steps of about 10°. Single-segment 19 events with an energy of 121.78±5 keV, corresponding to a strong gamma line of ^{152}Eu, were selected. The mean free path of such gammas is about 4 mm and the dominant interaction cross section is associated to the photo effect. Thus, most interactions create a single energy deposit close to the outer mantle.

Figure 14 shows the mean risetimes for (a) the core and (b) segment 19. Again, the difference is striking. While the core pulses show the normal small variation in risetime depending on their relative location to the crystal axes, the segment 19 pulses only show "normal" risetimes close to the metalisation. For locations far away from the metalisation, the risetimes are as large as for the alpha induced events. This proves that the effect of the missing metalisation is not confined to the very top of segment 19.

7. Conclusions

The observation of alpha events over most of the surface of the passivated end-plate of a true-coaxial detector was not really expected. It demonstrates that the inactive volume

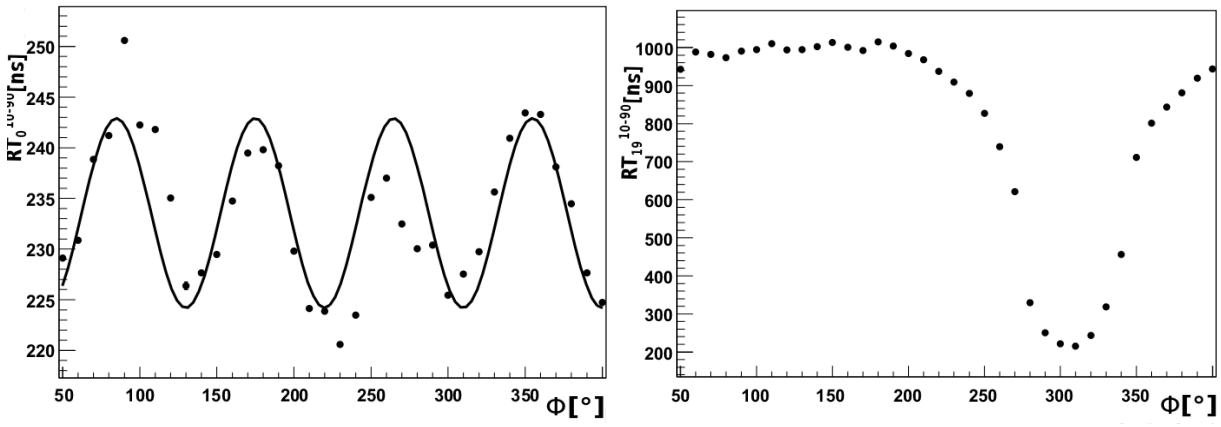

(a) (b)

Figure 14: The mean RT_i^{10-90} (a) for the core, $i = 0$, and (b) for segment 19, $i = 19$ as a function of ϕ as determined from a side-scan of the detector, adapted from [15].

underneath the passivation layer is extremely thin, only of the order of 10 μm thick. The spectra resulting for alpha interactions in the end-plate cover the region around 2 MeV where the signal for neutrinoless double beta decay would appear. If only the energy registered in core is recorded, such an alpha event could be mistaken for a signal event. A simple analysis of the shape of the core pulse would not help, because its risetime is normal.

In order to identify such events on the surface of an end-plate, it is necessary to read out the mantle. The difference between the energies recorded for the core and the mantle can tag alpha induced surface events.

Surface events are characterised by charge trapping, both of holes and electrons. However, to clearly identify these trapping effects, it is necessary to have the mantle segmented. This might not be favourable for a large scale experiment with hundreds of detectors. A possible handle might be a special configuration of the metalisation close to the end-plate. Contrary to intuition, it might be favourable to leave a small ring of the detector close to the end-plate without metalisation. A ring height of 5 mm is definitely too much because it affects an equally deep layer, but a ring height matching the volume to be tagged could help to identify events close to the end-plate through the slow rise of their mantle pulses.

Acknowledgements

We would like to thank the staff of Canberra France for their cooperation.

References

References

[1] I. Abt, et al., A New Ge^{76} Double Beta Decay Experiment at LNGS: Letter of Intent.arXiv:hep-ex/0404039.

[2] N. Abgrall, et al., The Majorana Demonstrator Neutrinoless Double-Beta Decay Experiment, Adv.High Energy Phys. 2014 (2014) 365432. arXiv:1308.1633, doi:10.1155/2014/365432.

[3] Neutrino 2016: First results from GERDA Phase II, http://neutrino2016.iopconfs.org/IOP/media/uploaded/EVIOP/event_948/09.25__5__agostini.pdf (2016).

[4] S. R. Elliott, et al., Initial Results from the MAJORANA DEMONSTRATOR, 2016. arXiv:1610.01210.
URL https://inspirehep.net/record/1489627/files/arXiv:1610.01210.pdf

[5] F. Feruglio, et al., Neutrino oscillations and signals in β and $0\nu\beta\beta$ experiments, Nucl. Phys. B637 (2002) 345. arXiv:hep-ph/0201291.

[6] W. Maneschg, Review of neutrinoless double beta decay experiments: Present status and near future, Nuclear and Particle Physics Proceedings 260 (2015) 188 – 193. doi:http://dx.doi.org/10.1016/j.nuclphysbps.2015.02.039.

[7] R. A. Johnson, T. H. Burritt, S. R. Elliott, V. M. Gehman, V. E. Guiseppe, J. F. Wilkerson, Alpha Backgrounds for HPGe Detectors in Neutrinoless Double-Beta Decay Experiments, Nucl. Instrum. Meth. A693 (2012) 51–58. arXiv:1201.0165, doi:10.1016/j.nima.2012.06.043.

[8] C. Aalseth, et al., CoGeNT: A Search for Low-Mass Dark Matter using p-type Point Contact Germanium Detectors, Phys.Rev. D88 (1) (2013) 012002. arXiv:1208.5737, doi:10.1103/PhysRevD.88.012002.

[9] K.-J. Kang, et al., Introduction to the CDEX experiment, Front.Phys.China 8 (2013) 412–437. arXiv:1303.0601, doi:10.1007/s11467-013-0349-1.

[10] F. Ruppin, J. Billard, E. Figueroa-Feliciano, L. Strigari, Complementarity of dark matter detectors in light of the neutrino background, Phys.Rev. D90 (8) (2014) 083510. arXiv:1408.3581, doi:10.1103/PhysRevD.90.083510.

[11] I. Abt, A. Caldwell, B. Dönmez, L. Garbini, S. Irlbeck, B. Majorovits, M. Palermo, O. Schulz, H. Seitz, F. Stelzer, The GALATEA Test-Facility for High Purity Germanium Detectors, Nucl. Instrum. Meth. A782 (2015) 56–62. arXiv:1409.0493, doi:10.1016/j.nima.2015.02.007.

[12] S. Irlbeck, The galatea test facility and a first study of α-induced surface events in a germanium detector, Phd thesis, Ludwig-Maximilians-Universität (March 2014).

[13] L. Garbini, Alpha-event characterization for germanium detectors, Phd thesis, Ludwig-Maximilians-Universität (May 2016).

[14] I. Abt, A. Caldwell, D. Gutknecht, K. Kroninger, M. Lampert, X. Liu, B. Majorovits, D. Quirion, F. Stelzer, P. Wendling, Characterization of the first true coaxial 18-fold segmented n-type prototype detector for the GERDA project, Nucl. Instrum. Meth. A577 (2007) 574–584. arXiv:nucl-ex/0701004, doi:10.1016/j.nima.2007.03.035.

[15] D. Lenz, Pulse shapes and surface effects in segmented germanium detectors, Phd thesis, Technische Universität München (March 2010).

[16] B. Majorovits, I. Abt, M. Laubenstein, O. Volynets, Aluminum as a source of background in low background experiments, Nucl. Instrum. Meth. A647 (2011) 39–45. arXiv:1105.3591, doi:10.1016/j.nima.2011.05.042.

[17] D. Gutknecht, private communication (2015).